4.10 Soil Moisture and Laser Intensity

This component of the analysis of LiDAR intensity data aimed to test the hypotheses that intensity values vary in relation to soil moisture. Soil moisture measurements were taken at significant locations within each of the geomorphological zones identified within the study area (i.e. modern floodplain, Holme Pierrepont Sand and Gravel and Hemington Sand and Gravel). Moisture readings were taken using a Delta T Devices PR2 profile probe attached to a ML2x ThetaProbe and HH2 soil moisture meter. The ThetaProbe measures *in-situ* volumetric soil moisture content to within 1%, removing the need to recover samples for laboratory and analysis. In conjunction with the PR2 profile probe the equipment is able to obtain moisture readings at different depths within a vertical soil profile (up to six sensors in the 100cm probe).

Moisture readings were taken at topsoil and subsoil depth (c 10cm and c 50cm) as it proved impossible to auger suitable holes for insertion of the profile probe to its full depth in the deposits across the study area. The project design envisaged recording soil moisture at the same locations at seasonal intervals, to determine average soil moisture for each location. In the event equipment supply difficulties prevented this, and a single set of moisture readings were collected in April 2005 at 35 sample points spread across the three major geomorphological zones within the study area (Fig. 4.37).

The location of each soil moisture reading was recorded using GPS, and location and moisture data combined and imported into ArcGIS 9. Using the GIS, LiDAR intensity values were extracted for each soil moisture sample location and these and the moisture values were combined using Microsoft Excel. Data for each geomorphological unit were then examined separately to test the relationship between LIDAR intensity and soil moisture

All data were standardised (by subtracting the mean and dividing by the standard deviation) and the standardised values used to produce scatter plots for each geomorphological zone (Fig. 4.38) as well as a graph showing variations in volumetric topsoil and subsoil moisture and LiDAR intensity within and across each geomorphological unit (Fig. 4.39). Basic correlation coefficients were calculated to describe the relationships between topsoil moisture, subsoil moisture and LiDAR intensity within each geomorphological zone. In addition, variations in soil moisture and intensity were represented graphically as bar graphs superimposed on the LiDAR intensity image within ArcGIS (Fig. 4.40).

There appears to be a strong negative correlation between LiDAR intensity and soil moisture. The variations appear consistent within geomorphological and across geomorphological zones, although moisture and intensity values between zones vary too widely for meaningful comparison. For example, areas of low soil moisture on the higher gravels of terrace 2, while exhibiting a relatively low LiDAR intensity compared to terrace 1 and the modern floodplain (possibly because of vegetation differences) nonetheless display a consistent inverse relationship to soil moisture levels within the unit. Likewise, on the modern floodplain, where LiDAR intensity levels are significantly higher than on terrace 2, variations in intensity are still reflected by corresponding inverse variations in soil moisture.

The correlation coefficients for each geomorphological zone are tabulated below (Tab. 4.3).

MF (alluvium)	Topsoil Moisture and LiDAR Intensity = -0.741
	Subsoil Moisture and LiDAR Intensity = -0.541
T1 (Hemington)	Topsoil Moisture and LiDAR Intensity = -0.926

Subsoil Moisture and LiDAR Intensity = -0.589

T2 (Holme Pierrepont) Topsoil Moisture and LiDAR Intensity = -0.815
Subsoil Moisture and LiDAR Intensity = -0.219

Tab 4.3: Tabulated coefficients of correlation between volumetric moisture of topsoil, subsoil and LiDAR Intensity for each geomorphological zone.

In each case there is a strong inverse relationship between topsoil moisture levels and LiDAR intensity and a less pronounced inverse relationship between subsoil moisture and intensity. The geographically determined nature of these variations is effectively illustrated (Fig. 4.39), where examination of the bar graphs shows that, whatever the absolute levels of soil moisture and intensity, variations are linked to geomorphological features. For example within terrace 1, soil moisture increases where measured within a palaeochannels and LiDAR intensity shows a corresponding decrease. Given the limited data gathered to date it is not possible to demonstrate statistically sound relationships between soil moisture and intensity. Nevertheless, the results to date show promise and suggest that further work gathering more soil moisture data at different seasons, and to examine the effect of variations in soil moisture at depth, may yield significant results.

Sample No	Topsoil Moisture %	Subsoil Moisture %	LiDAR Intensity	Topsoil Standardised	Subsoil Standardised	Intensity Standardised
12	16.90	27.20	42.329830	-2.270541	-0.519756	-0.637927
13	28.20	30.40	28.613565	-1.332487	-0.256589	-1.407291
14	26.60	31.60	30.947359	-1.465309	-0.157901	-1.276386
15	25.10	21.90	35.837856	-1.589829	-0.955628	-1.002071
16	26.70	18.00	36.932568	-1.457007	-1.276363	-0.940667
17	29.50	27.80	30.221449	-1.224569	-0.470412	-1.317103
18	25.80	18.20	28.560318	-1.531719	-1.259915	-1.410278
19	28.50	32.70	31.434139	-1.307583	-0.067437	-1.249081
20	33.50	27.50	45.617989	-0.892515	-0.495084	-0.453489
21	40.00	26.50	25.966194	-0.352926	-0.577324	-1.555786
22	34.90	20.10	57.494923	-0.776296	-1.103660	0.212705
23	47.50	45.80	84.856277	0.269676	1.009906	1.747442
24	48.30	41.00	81.069893	0.336086	0.615154	1.535059
26	47.10	25.30	74.904305	0.236470	-0.676012	1.189222
27	43.70	40.20	83.392311	-0.045776	0.549363	1.665326
28	50.00	45.60	85.998024	0.477210	0.993458	1.811484
29	50.60	43.20	75.255852	0.527018	0.796082	1.208941
30	60.50	50.40	50.312374	1.348852	1.388210	-0.190174
31	60.70	58.10	56.597992	1.365455	2.021457	0.162395
32	60.20	54.60	47.744099	1.323948	1.733617	-0.334233
33	53.70	40.60	54.018414	0.784360	0.582259	0.017703
34	50.90	45.40	54.869591	0.551922	0.977010	0.065446
35	52.70	45.20	30.498705	0.701346	0.960562	-1.301551
36	56.20	42.60	52.512970	0.991894	0.746738	-0.066740
37	53.20	22.50	53.989609	0.742853	-0.906284	0.016087
38	47.80	36.50	65.945023	0.294580	0.245075	0.686683
39	49.90	7.60	59.758495	0.468908	-2.131658	0.339672
40	49.40	32.40	67.582253	0.427401	-0.092109	0.778518
41	50.20	43.40	64.621849	0.493812	0.812530	0.612464
42	49.20	24.90	64.307289	0.410799	-0.708908	0.594820
43	47.10	38.50	61.494431	0.236470	0.409555	0.437043
44	45.80	27.70	67.691284	0.128552	-0.478636	0.784633
45	45.10	18.80	51.081062	0.070443	-1.210571	-0.147058
46	48.30	14.80	61.208416	0.336086	-1.539531	0.421000
47	65.00	46.20	35.931637	1.722414	1.042802	-0.996810

Tab 4.4: Tabulated volumetric soil moisture and corresponding LiDAR intensity data also showing standardised values.

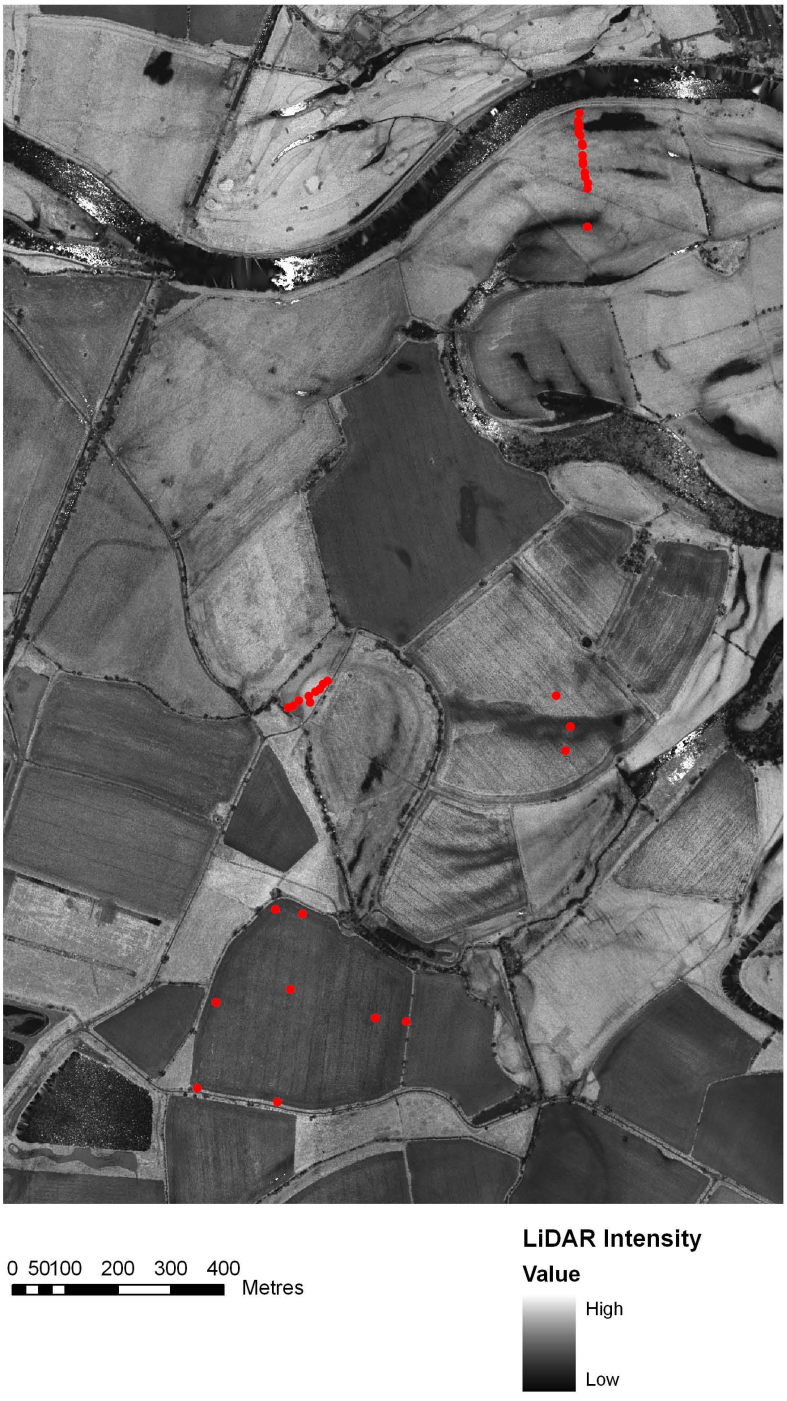

Fig 4.37: LiDAR intensity data for the study area with the locations of *in-situ* volumetric soil moisture readings shown in red.

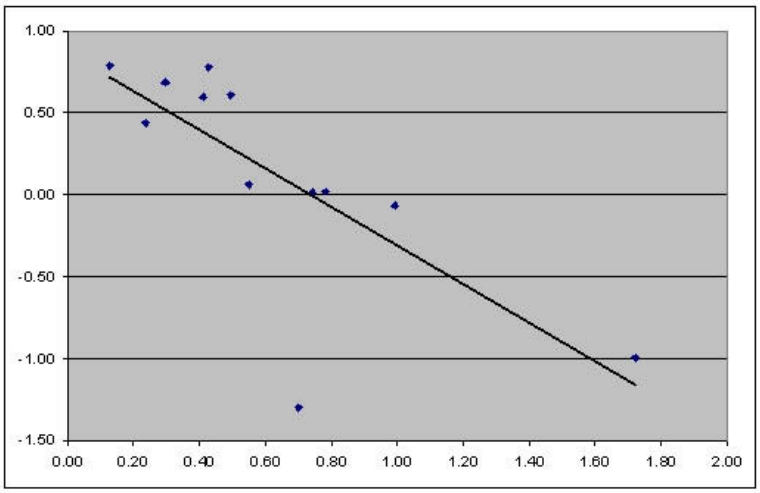

Modern Floodplain

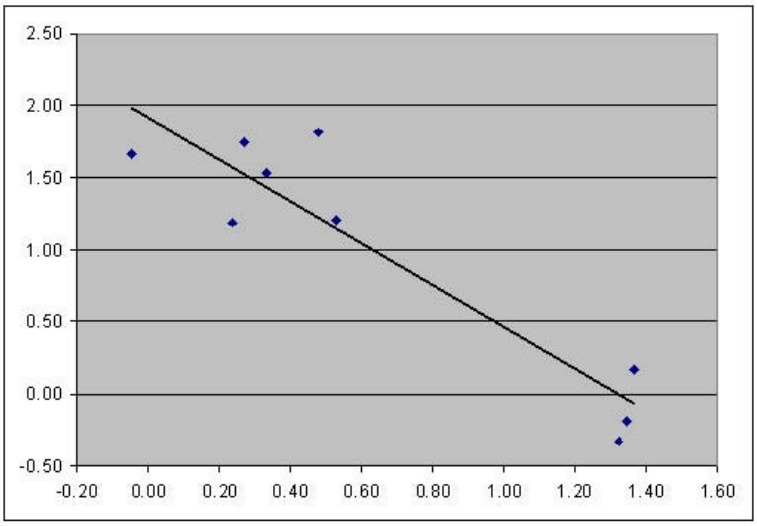

Terrace 1 (Hemington)

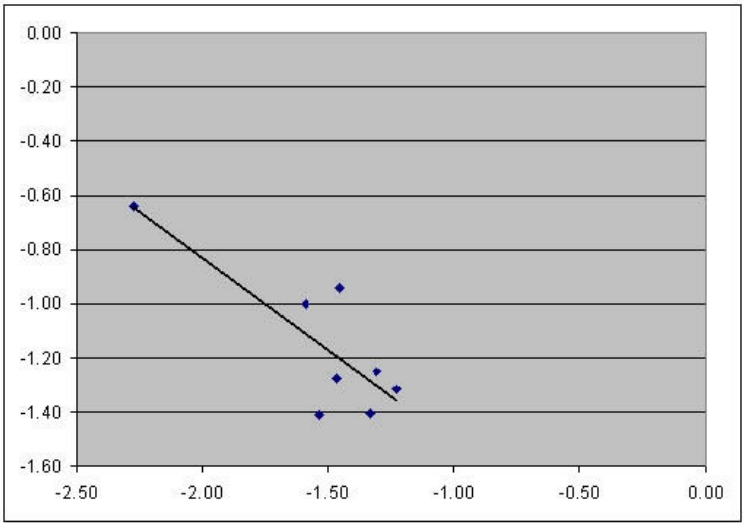

Terrace 2 (Holme Pierrepont)

Fig 4.38: Scatter plots with fitted trend lines showing the relationship between topsoil moisture and LiDAR intensity in each geomorphological zone. In each graph x axis is soil moisture y axis is LiDAR intensity. Units are standard deviation.

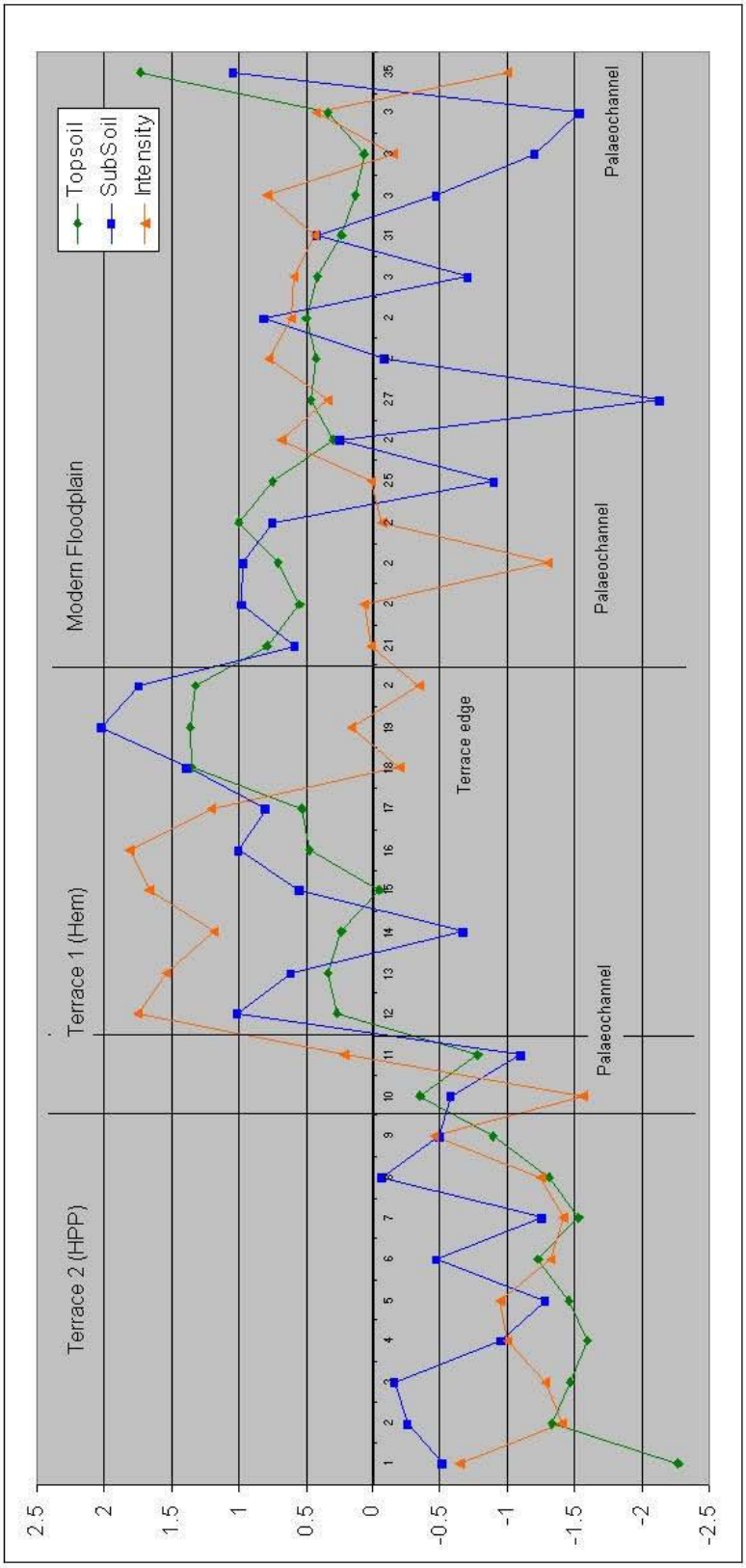

Fig 4.39: Line graph showing standardised variations in volumetric soil moisture in the topsoil (green), subsoil (blue) and LiDAR laser intensity (orange) at ach sample location, vertical bars indicate the boundaries between geomorphological units, annotations indicate geomorphological features. Graph axes are in units of standard deviation.

Terrace 2 (Holme Pierrepont)

Terrace 1 (Hemington)

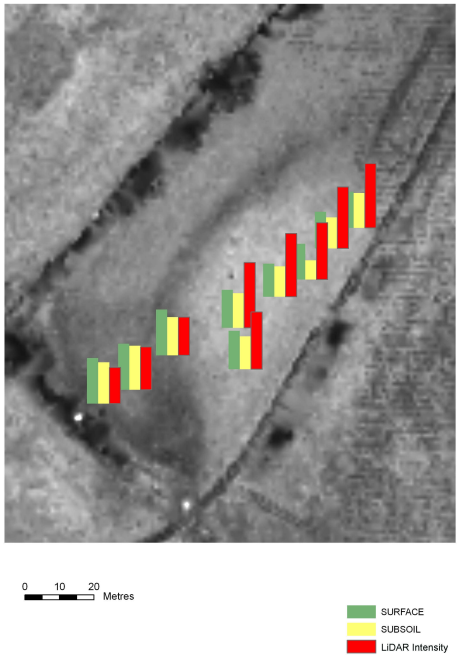

Terrace 1 (Hemington)

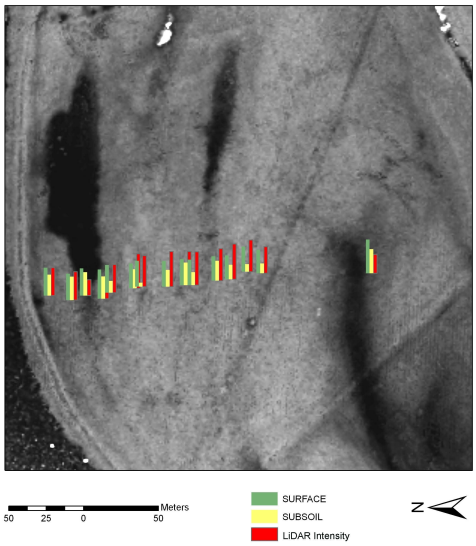

Modern floodplain

Fig 4.40: Maps showing LiDAR intensity with superimposed bar charts showing volumetric soil moisture readings at the surface (green) at subsoil level (yellow) and corresponding LiDAR intensity value at sample locations 1-4.

4.11 Inteferometric Synthetic Aperture Radar

Airborne radar uses radio waves to measure the distance between an aircraft mounted senor and the ground surface. Interferometry relies on picking up the returned radar signal using antennas at two different locations. Each antenna collects data independently, although the information they receive is almost identical, with little separation (parallax) between the two radar images. Instead the phase difference between the signals received by each of the two antennas is used as a basis for calculation changes in elevation. The results are enhanced by using processing techniques during data collection to generate a synthetic aperture of much greater size than the physical antenna used and so enhance resolution (Intermap 2003). Combining the principals of Synthetic Aperture Radar with Interferometry, Interferometric Synthetic Aperture Radar (IFSAR) is capable of producing both a radar image of the ground surface and calculating elevation changes to enable production of a digital surface model (DSM).

Intermap has undertaken IFSAR surveys of the entire of the UK. The results of the surveys are available as a commercial product in the form of 5m spatial resolution DSM with a vertical accuracy of between 0.5 and 1.0m and a 1.25m spatial resolution radar image. Analysis of the IFSAR products focused on investigating to what extent they were able to provide useful geoarchaeological information. The IFSAR DSM was imported into ArcGIS for visualisation and comparison with LiDAR and GPS derived elevation values. Elevation and derived slope frequency histograms were generated as well as basic DSM statistics (Fig. 4.43, Tab. 4.5). Profiles across the IFSAR DSM were generated at each location used to assess LIDAR DSM accuracy and resolution (Fig. 4.17) to allow direct comparison of the resolving ability of the IFSAR DSM compared to LiDAR. Finally, a crude approximation of the variation in elevation values reported by the IFSAR DSM as compared to LIDAR was produced by subtracting elevation values for the LiDAR first pulse DSM from those for the IFSAR DSM (Fig. 4.44).

4.11.1 IFSAR DSM

In general the IFSAR DSM is successful in distinguishing the broad geomorphological units of the study area, in particular the elevation changes between the Holme Pierrepont (T2) and Hemington (T1) terraces and the modern floodplain (Fig. 4.41). Profiles across the study area (Fig. 47) show that the broad changes in elevation that distinguish these units are recorded by the IFSAR DSM. However, IFSAR provides a relatively poor record of the subtle microtopographic features that are the basis of mapping and understanding floodplain and terrace geomorphology. While it is possible to distinguish a number of the palaeochannels evident on LiDAR and air photographic imagery in the IFSAR DSM, these are not represented with anywhere near the clarity seen in the LiDAR data. Close comparison of profiles through the IFSAR DSM at key geomorphological features (Figs. 4.18 – 4.23) show that the 10m resolution of the IFSAR data, though able to distinguish features is not able to adequately represent their form, thus ridge and swale is rendered as a series of crude stepped ridges (Fig. 4.18, P1) and palaeochannels profiles are similarly crudely represented (see especially Fig. 4.18, P2 and Figure P3 and 4). Some features, such as the terrace edge in Fig. 4.20, P6) are not represented at all, and in areas of low relief, especially the modern floodplain, results are wholly unreliable (Figs. 4.21 – 4.23).

Finally, comparison of the elevation values reported by the IFSAR and LiDAR FP DSM show some variations between the two products (Figs. 4.42 and 4.44). The majority of variations are in areas of vegetation cover and a probably a product of the differing technologies ability of represent and penetrate vegetation, as well as variations in the actual vegetation canopy at the times of the two survey flights.

4.11.2 IFSAR ORI

Radar imagery responds largely to changes in the texture of the land surface and so records different land surface properties to both conventional aerial photography and LiDAR laser intensity information. ORI data was compared with other sources of information about the ground surface in the study area to test its utility in identifying significant floodplain features. The IFSAR ORI provides a fair overall representation of the study area (Fig. 4.45), but fails comprehensively to detect the significant geomorphological features. Close comparison of extracts from the ORI with air photo and LiDAR data (Fig. 4.46, compare with Figs. 4.15, 4.16 and 4.32) indicate that although some crude variations in texture, corresponding to subsoil variations and geomorphological features, are evident, the resolution and reliability of the ORI for detecting such features is poor. The IFSAR ORI does not contribute significantly to the geoarchaeological investigation of the study area and its further investigation cannot be recommended.

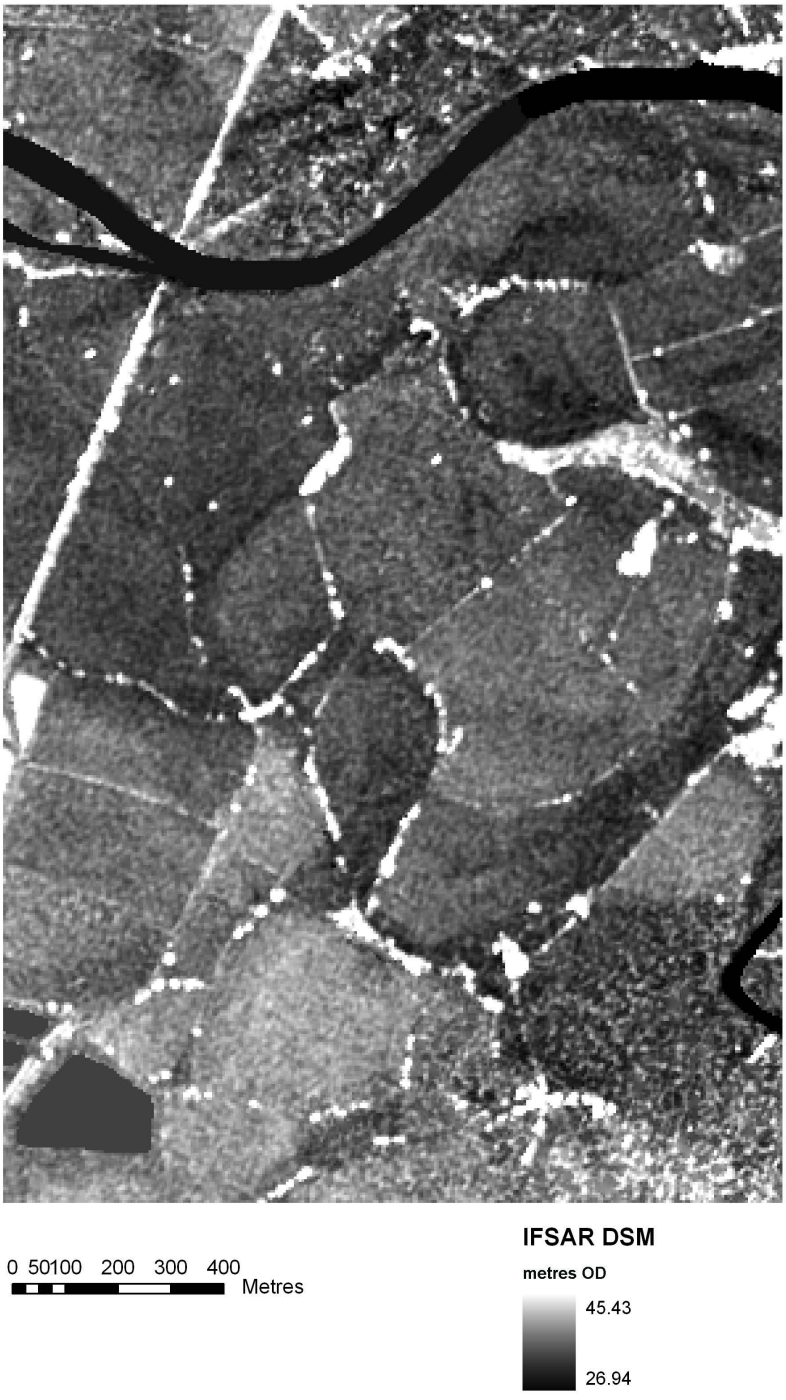

Fig 4.41: IFSAR (Radar) 10m digital surface model of the study area.

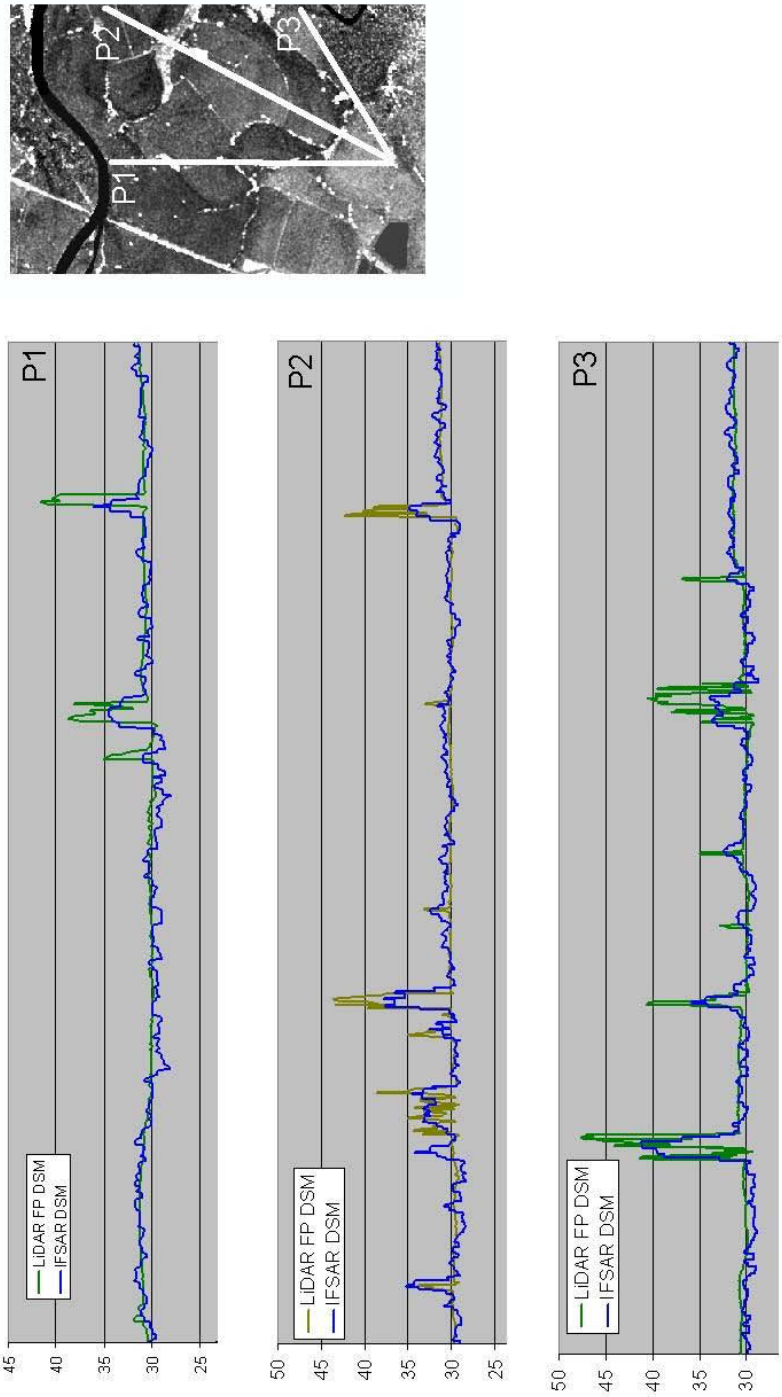

Fig 4.42: Profiles through the LiDAR and IFSAR DSM of the study area showing the elevation of the major geomorphological units.

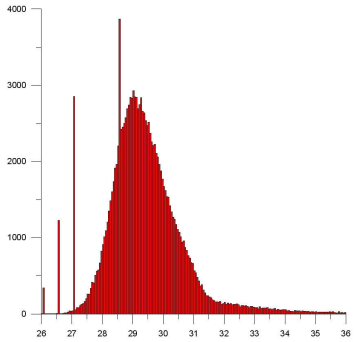

IFSAR 10m DSM

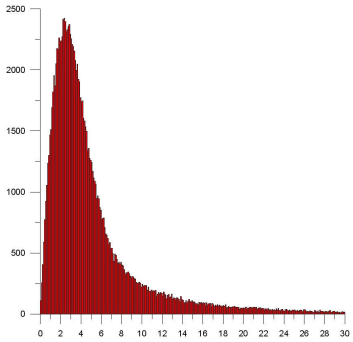

IFSAR 10m Slope

Fig 4.43: Left elevation and right slope for IFSAR DSM data for the entire study area.

DSM IFSAR	
Number of values	133930
Minimum	26.94
Maximum	45.44
Range	18.5
Mean	30.357
Standard deviation	1.3921
Skew	2.029
Slope IFSAR	
Number of values	133930
Minimum	0
Maximum	57.36
Range	57.36
Mean	5.0564
Standard deviation	5.2662
Skew	2.844

Tab 4.5: Statistics for the IFSAR DSM and derived slope values.

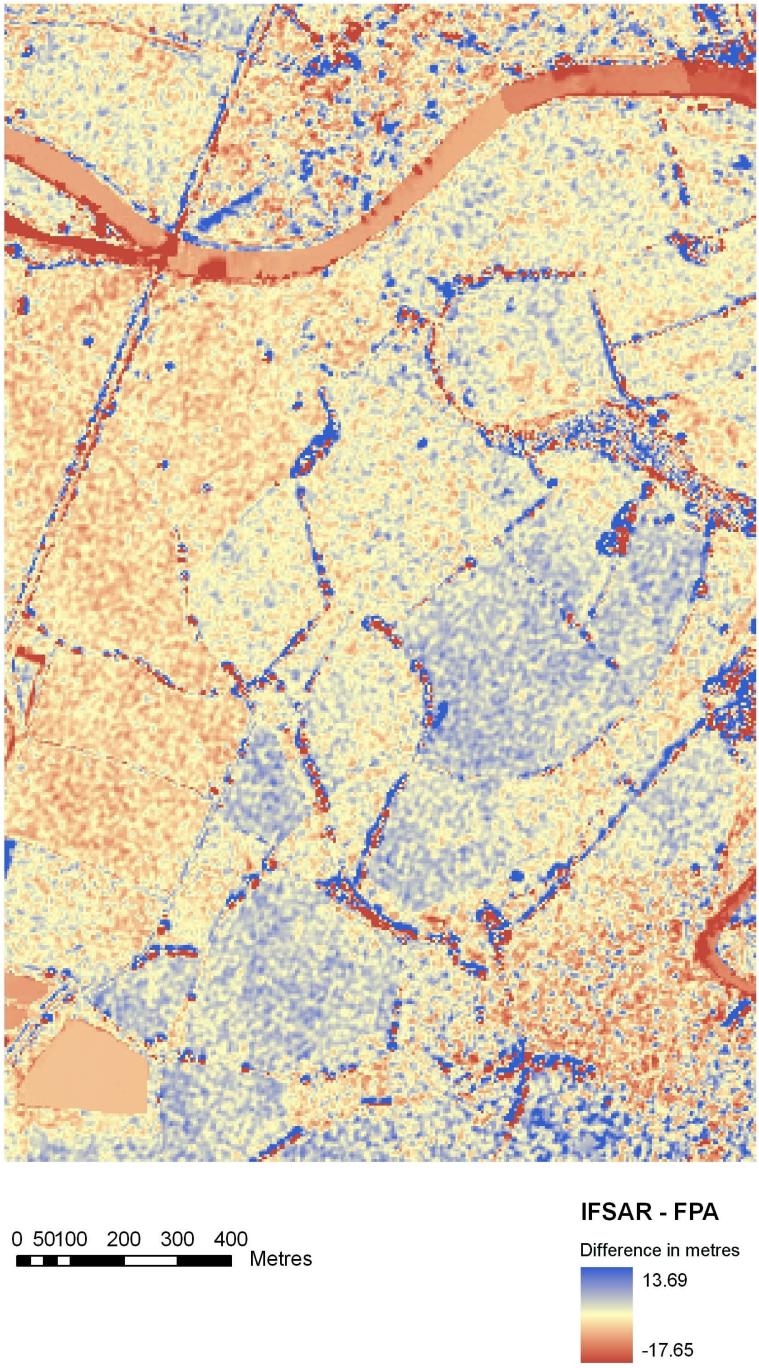

Fig 4.44: Difference between elevation values recorded by the IFSAR (Radar) 10m digital surface model of the study area and the LiDAR first pulse surface model.

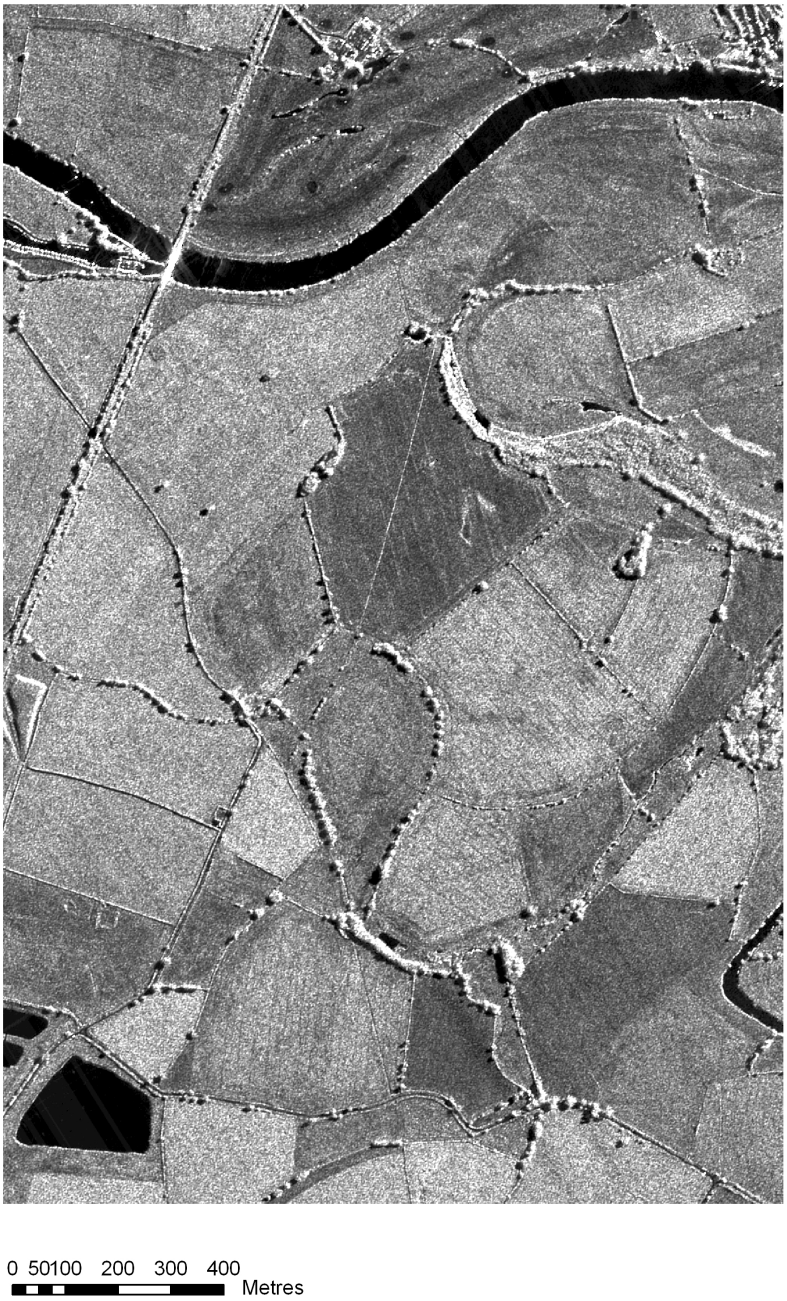

Fig 4.45: IFSAR (Radar) Orthorectified Radar Image (ORI) of the study area.

Modern Floodplain (compare fig. 15)

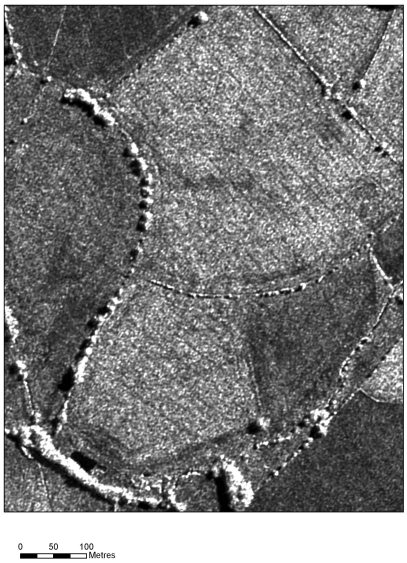

Terrace 1 (compare fig.16)

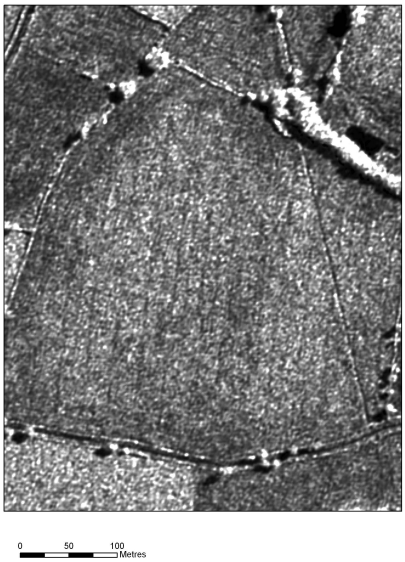

Terrace 2 (Lockington villa: compare fig. 32)

Fig 4.46: IFSAR ORI of selected parts of the study area.